CrossMark

Real-Time Amplitude and Phase Imaging of Optically Opaque Objects by Combining Full-Field Off-Axis Terahertz Digital Holography with Angular Spectrum Reconstruction

Masatomo Yamagiwa[1,2] · Takayuki Ogawa[3] ·
Takeo Minamikawa[1,2] · Dahi Ghareab Abdelsalam[1,2,4] ·
Kyosuke Okabe[5] · Noriaki Tsurumachi[5] ·
Yasuhiro Mizutani[2,6] · Testuo Iwata[1,2] ·
Hirotsugu Yamamoto[2,7] · Takeshi Yasui[1,2]

Abstract Terahertz digital holography (THz-DH) has the potential to be used for non-destructive inspection of visibly opaque soft materials due to its good immunity to optical scattering and absorption. Although previous research on full-field off-axis THz-DH has usually been performed using Fresnel diffraction reconstruction, its minimum reconstruction distance occasionally prevents a sample from being placed near a THz imager to increase the signal-to-noise ratio in the hologram.

✉ Takeshi Yasui
yasui.takeshi@tokushima-u.ac.jp

1 Graduate School of Technology, Industrial and Social Sciences, The Tokushima University, 2-1, Minami-Josanjima, Tokushima 770-8506, Japan

2 JST, ERATO, MINOSHIMA Intelligent Optical Synthesizer Project, 2-1, Minami-Josanjima, Tokushima 770-8506, Japan

3 Graduate School of Advanced Technology and Science, The Tokushima University, 2-1, Minami-Josanjima, Tokushima 770-8506, Japan

4 Engineering and Surface Metrology Lab, National Institute of Standards, Tersa St., El Haram, El Giza 12211, Egypt

5 Faculty of Engineering, Kagawa University, 2217-20, Hayashicho, Takamatsu, Kagawa 761-0396, Japan

6 Graduate School of Engineering, Osaka University, 2-1, Yamadaoka, Suita, Osaka 565-0871, Japan

7 Center for Optical Research and Education, Utsunomiya University, 7-1-2, Yoto, Utsunomiya, Tochigi 321-8585, Japan

In this article, we apply the angular spectrum method (ASM) for wavefront reconstruction in full-filed off-axis THz-DH because ASM is more accurate at short reconstruction distances. We demonstrate real-time phase imaging of a visibly opaque plastic sample with a phase resolution power of $\lambda/49$ at a frame rate of 3.5 Hz in addition to real-time amplitude imaging. We also perform digital focusing of the amplitude image for the same object with a depth selectivity of 447 μm. Furthermore, 3D imaging of visibly opaque silicon objects was achieved with a depth precision of 1.7 μm. The demonstrated results indicate the high potential of the proposed method for in-line or in-process non-destructive inspection of soft materials.

Keywords Terahertz · Digital holography · Phase image · Off-axis · Angular spectrum method

1 Introduction

Digital holography (DH) [1] is a technique that acquires a hologram of an object by a digital imaging device and numerically reconstructs the optical wavefront based on the acquired hologram to obtain both the amplitude and phase images of the sample object. Furthermore, the phase image can be used for three-dimensional (3D) imaging of geometrical shapes or optical thicknesses in an object with a sub-wavelength depth resolution, whereas digital focusing of the amplitude image [2] enables 3D imaging with a wavelength depth resolution over a wide dynamic range of depths without changing the optical system. Until now, visible light has been widely used for DH with a variety of light sources and digital imaging devices, namely, VIS-DH. The 3D shape of a visibly transparent object can be visualized by VIS-DH in a transmission configuration [3]. Furthermore, the VIS-DH reflection configuration enables 3D imaging of surface shapes in a visibly opaque object [4]. Due to its real-time, quantitative, 3D-imaging capability, VIS-DH has been widely used in various applications in science and industry.

However, if the object surface is visibly rough, strong scattering and/or phase wrapping ambiguity will be problematic in VIS-DH. Additionally, transmission VIS-DH cannot be applied to a visibly opaque object. If DH is performed using other electromagnetic radiation with good immunity to optical scattering and good penetration of visibly opaque objects, the applications of DH will be further expanded; for example, non-destructive inspection of soft materials, such as plastics, semiconductor, ceramics, rubber, wood, and concrete, will be realized.

One promising radiation for this purpose is terahertz (THz) radiation (freq. = 0.1~10 THz, wavelength = 30~3000 μm) [5, 6]. Due to its existence at the boundary between optical and electric radiation, THz radiation has both characteristics, i.e., good penetration of visibly opaque, non-metallic materials, less scattering by visibly rough surfaces or visible scattering objects, good beam coherence, low invasiveness, and multiple spectral fingerprints. Fortunately, the recent progress of continuous-wave (CW) THz laser sources and THz digital imagers allows full-field DH to be easily performed in the THz region [7–16]. For example, the combination of a gas far-infrared laser with a pyroelectric array detector was applied for Garbor-type in-line transmission THz-DH to acquire the phase image of cancerous tissues [12]. While in-line THz-DH can be performed in a simple optical configuration without the need of a two-arm interferometer, it is hampered by the spatial overlap of unnecessary zero-order-diffraction-light and conjugate first-order-diffraction-light images on the necessary first-order-diffraction-light image. To overcome this problem, off-axis full-field THz-DH [13] was performed in a transmission or reflection configuration using a THz quantum cascade laser

(THz-QCL) [17, 18] and uncooled, bolometer-type 2D focal plane array [19]; in this case, the unnecessary zero-order-diffraction-light and conjugate first-order-diffraction-light images were spatially separated and then filtered in the spatial frequency domain. By using the Fresnel diffraction method (FDM) [20, 21] for the numerical reconstruction of the THz wavefront, the THz amplitude and phase imaging of the samples was demonstrated in real time. While FDM performs only one Fourier transform, its use is limited under certain conditions, e.g., the minimum distance (reconstruction distance z) between the object plane and the hologram plane. In many cases of actual full-field THz-DH, the output power of a THz-QCL is not always enough to achieve a high signal-to-noise ratio (SNR) in a real-time hologram acqui-sition by a THz digital imager; in this case, the object must be placed near the imager to reduce the signal loss in the lens-less configuration of DH. Such an experimental configuration may not satisfy the requirement for the minimum z in FDM. An angular spectrum method (ASM) [20, 21] is another hologram reconstruction method and is more accurate for short reconstruc-tion distances; however, a Fourier transform is performed twice. ASM has been used for point-scanning THz-DH systems [7, 15], but no attempt has been made to use ASM in full-field THz-DH equipped with THz-QCL and THz digital imagers.

In this article, we acquired a THz digital hologram using a full-field off-axis THz-DH system equipped with THz-QCL and uncooled, bolometer-type 2D focal plane arrays and then, performed the numerical reconstruction of the wavefront based on ASM. Furthermore, we evaluated the phase noise in the reconstructed phase image, which limits the precision of the phase imaging and the 3D imaging of a sample. Finally, we demonstrated the quantitative phase imaging of visibly opaque objects in real time and the 3D shape measurement of a visibly opaque, stepped structure.

2 Method

2.1 Experimental Setup

Figure 1 illustrates a schematic diagram of a full-field off-axis THz-DH system in a transmis-sion configuration. The CW-THz radiation was generated by a THz-QCL (EasyQCL, LongWave Photonics LLC, center frequency = 3 THz, center wavelength = 100 μm, average power = 1.78 mW). The THz-QCL was kept at 50 K in a cryostat using a Stirling cycle cooler without the need for cryogenic cooling. After passing through an optical chopper (OC, 3501, New Focus, modulation frequency = 7.5 Hz), the CW-THz radiation was collimated at a diameter of 7 mm by an off-axis parabolic mirror (OA-PM, off-axis angle = 90°, diameter = 25.4 mm, focal length = 50.8 mm) and was fed into a Mach-Zehnder interferometer. In the interferometer, the object beam passed through a silicon beam splitter (BS, diameter = 101.6 mm, thickness = 500 μm, reflection = 54%, transmittance = 46%) and a sample, whereas the reference beam was reflected by BS and an aluminum mirror (M). Both beams were incident onto an uncooled, 2D micro-bolometer array, namely, the THz imager (IRV-T0831, NEC Inc., sensor area = 7.52 mm × 5.64 mm, pixel number = 320 pixels × 240 pixels, pixel size = 23.5 μm × 23.5 μm, frame rate = 7.5 frames per second, exposure time = 66.7 ms, digital output resolution = 14 bit) at an off-axis angle of 40°. This results in the generation of vertical interference patterns of CW-THz radiation on the THz imager, namely, the THz digital hologram. To improve the image SNR, we adopted a dynamic subtraction technique by synchronizing the THz imager with the CW-THz radiation. To this end, the CW-THz radiation

was chopped with the OC. We performed alternating acquisitions of the image with and without the CW-THz radiation and subtracted successive images, thereby suppressing the background noise. The minimum sampling spacing in the THz hologram is 47 μm from the sampling theorem for a THz imager with a 23.5-μm pixel pitch.

2.2 Hologram Reconstruction

ASM is a method to directly calculate the diffraction integral. Since the details of ASM are given elsewhere [20, 21], we briefly describe the main characteristics of this method. In the scalar diffraction theory, the diffracted field, $\psi_p(x, y; z)$, is given by the incident field, $\psi_{p0}(x, y)$, as follows:

$$\psi_p(x, y; z) = F^{-1}\langle F\{\psi_{p0}(x, y)\} \times H(k_x, k_y; z)\rangle, \tag{1}$$

where $H(k_x, k_y; z)$ is the spatial frequency transfer function (SFTF). As shown in Eq. (1), ASM requires two Fourier transform (FT) calculations. Assuming that the sampling period along the x-axis is Δ_x with a total of M samples and the sampling period along the y-axis is Δ_y with a total of N samples, the discrete form of Eq. (1) is given by:

$$\psi_p[m, n] = IDFT_{2D}\langle DFT_{2D}\{\psi_{p0}(m, n)\} \times H[p, q]\rangle. \tag{2}$$

In Eq. (2), the discrete form of SWTF, $H[p, q]$, is given by:

$$H[p, q] = e^{-jk_0 z \sqrt{1 - \frac{\left(p\Delta_{k_x}\right)^2}{k_0^2} - \frac{\left(q\Delta_{k_y}\right)^2}{k_0^2}}}, \tag{3}$$

where Δ_{kx} and Δ_{kx} are the frequency resolution corresponding to sampling periods, Δ_x and Δ_y, along the x- and y-directions, respectively. The sampling period of the reconstructed image is equal to that of the hologram regardless of the reconstruction distance.

3 Results

3.1 Amplitude and Phase Imaging of a Plastic Object

We first measured a plastic object, i.e., a visibly opaque sample with a 3D shape. In this sample, two letters, "P" and "S," were impressed in a convex manner (height = 228 μm)

Fig. 1 Experimental setup. *THz-QCL* THz quantum cascade laser (center frequency = 3 THz, average power = 1.78 mW); *OC* optical chopper (modulation freq. = 7.5 THz); *OA-PM* off-axis parabolic mirror (off-axis angle = 90°, diameter = 25.4 mm, focal length = 50.8 mm); *M* aluminum mirror; *BS* silicon beam splitter (diameter = 101.6 mm, thickness = 500 μm)
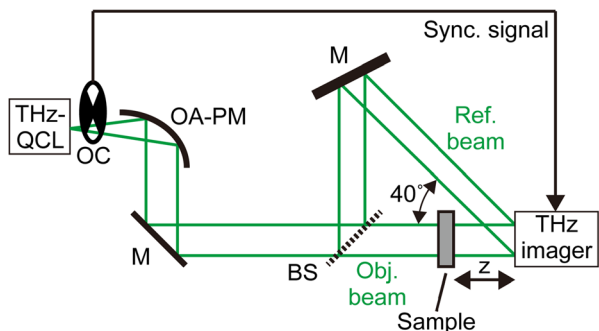
on a polystyrene plate (thickness = 0.8 mm, refractive index = 1.67), as shown in Fig. 2a. Figure 2b shows the acquired hologram (image size = 7.52 mm × 5.64 mm, pixel number = 320 pixels × 240 pixels, number of image integrations = 128). We confirmed the interference pattern with a spacing of ≈ 80 μm. This spacing was in good agreement with the expected value based on the CW-THz radiation wavelength of 100 μm and the off-axis angle of 40°. To avoid aliasing in the reconstruction, we added null data to the area around the hologram to increase the number of pixels to 640 pixels × 640 pixels. Then, we reconstructed the amplitude and phase images of the sample at a reconstruction distance, z, of 7 mm using ASM, as shown in Fig. 2c, d. The two letters "P" and "S" were clearly confirmed in both images. In the amplitude image, the image contrast is given by the edges of the letters due to the reflection and scattering losses of CW-THz radiation. However, the contrast in the phase image is due to the differences in the optical thickness in the letter and no letter regions. The phase image has a better contrast than the amplitude image in the limited SNR of the hologram.

We next demonstrated the digital focusing of the amplitude image in the same plastic sample (see Fig. 2a) by changing the reconstruction distance, z. Figure 3 and Video 1 show a series of amplitude images as z was changed at intervals of 1 mm (image size = 7.52 mm × 5.64 mm, pixel number = 320 pixels × 240 pixels, number of image integrations = 128). The letters "P" and "S" were in focus at $z = 7$ mm, but they were out of focus at $z \geq 8$ mm and ≤ 6 mm. The depth resolution of the digital focusing was estimated by the depth of the focus, DF, of the optical system as follows:
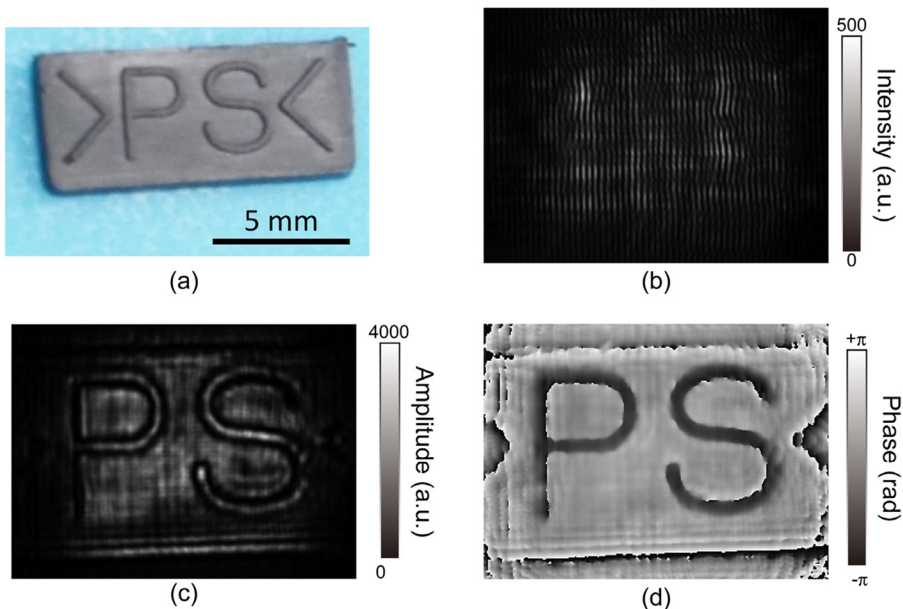
Fig. 2 a Optical photograph of a visibly opaque, plastic sample with two impressed letters, "P" and "S." b THz digital hologram (image size = 7.52 mm × 5.64 mm, pixel number = 320 pixels × 240 pixels, number of image integrations = 128). Reconstructed images of the c amplitude and d phase (image size = 7.52 mm × 5.64 mm, pixel number = 320 pixels × 240 pixels) by ASM

$$DF = \frac{\lambda}{NA^2} = \frac{100 \times 10^{-6}}{0.473^2} = 447 \ \mu\text{m}. \tag{4}$$

This depth resolution is reasonably reflected in Fig. 3 and Video 1. Because digital focusing does not require any changes in the optical setup, it is a powerful modality for 3D imaging over a wide dynamic range of depths. For example, if another object is placed at a different depth position, digital focusing allows us to individually separate and visualize them.

We also obtained a real-time movie of the amplitude and phase when the plastic sample (see Fig. 2a) was screened by a paper sheet. A hologram was acquired over 11.4 s at a frame rate of 3.5 Hz, as shown in the left panel of Video 2. Figure 4a shows a snapshot of the hologram movie (image size = 7.52 mm × 5.64 mm, pixel number = 320 pixels × 240 pixels, no image integration). The interference pattern was still observed in the single-shot hologram. By applying ASM to the full movie of the hologram, we obtained movies of both the amplitude and phase, as shown in the center and right panels of Video 2, respectively. Figure 4b, c shows snapshots of the amplitude and phase movies (image size = 7.52 mm × 5.64 mm, pixel number = 320 pixels × 240 pixels, reconstruction distance $z = 7$ mm) before the sample was screened by the paper sheet ($t = 0.285$ s). The two letters "P" and "S" were confirmed in both images. Next, Fig. 4d, e shows snapshots of the amplitude and phase movies when the sample was partially screened by the paper sheet ($t = 1.710$ s). Good contrast was still maintained in the phase image, whereas the two letters almost disappeared in the amplitude image due to the decreased amplitude caused by the paper sheet. These movies and figures reflect the change in the amplitude and phase caused by inserting the paper sheet in front of the sample. Further-more, the phase image is more powerful than the amplitude image in the low SNR. The real-time imaging capability of both the amplitude and phase has the potential to expand the applications of THz-DH.

3.2 3D Imaging of a Semiconductor Object Based on a Phase Image

We measured a semiconductor object, i.e., a visibly opaque sample with known 3D dimensions to demonstrate the potential for 3D imaging of visibly opaque objects. A checker pattern was carved on a silicon substrate (n-type, thickness = 300 μm, electric resistivity > 1 Ω•cm) by a photolithography method. Figure 5a shows the optical photo-graph and schematic drawing of the checker-patterned sample (grid size = 1 mm by 1 mm). The depth of the sample was determined to be 21.11 ± 0.03 μm by a 3D optical microscope based on white light interferometry (Veeco, Wyko NT9100, depth resolution < 0.1 nm, lateral resolution > 0.5 μm).

We acquired the THz digital hologram (see Fig. 5b, image size = 7.52 mm × 5.64 mm, pixel number = 320 pixels × 240 pixels, number of image integrations = 128) of the sample. By applying ASM to the acquire hologram, we reconstructed the amplitude image and phase image of the sample (image size = 7.52 mm × 5.64 mm, pixel number = 320 pixels ×240 pixels) at a reconstruction distance, z, of 7 mm, as shown in Fig. 5c, d. In the amplitude image, although the edge of the grid pattern was confirmed, the checker pattern with different thicknesses was not as clear due to the small differences in the THz attenuation between the checker patterns. However, the phase image clearly shows the checker pattern due to the large difference in the optical thicknesses of the top and bottom surfaces.
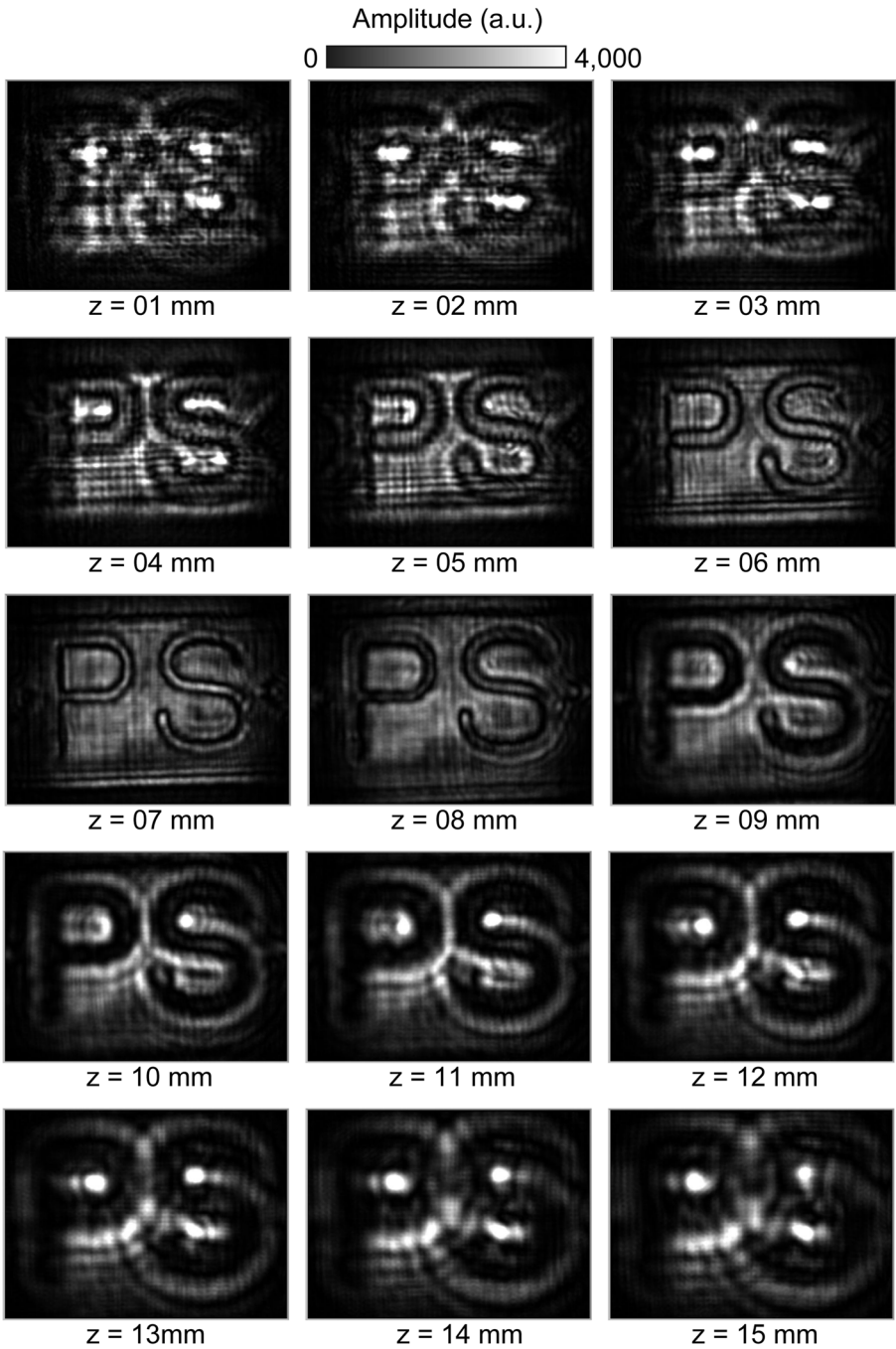
Fig. 3 Digital focusing of the amplitude image (image size = 7.52 mm × 5.64 mm, pixel number = 320 pixels × 240 pixels, number of image integrations = 128) for visibly opaque, plastic sample (see Fig. 2a) by ASM. The reconstruction distance, z, was changed at intervals of 1 mm within a range of 15 mm. The corresponding movie is Video 1
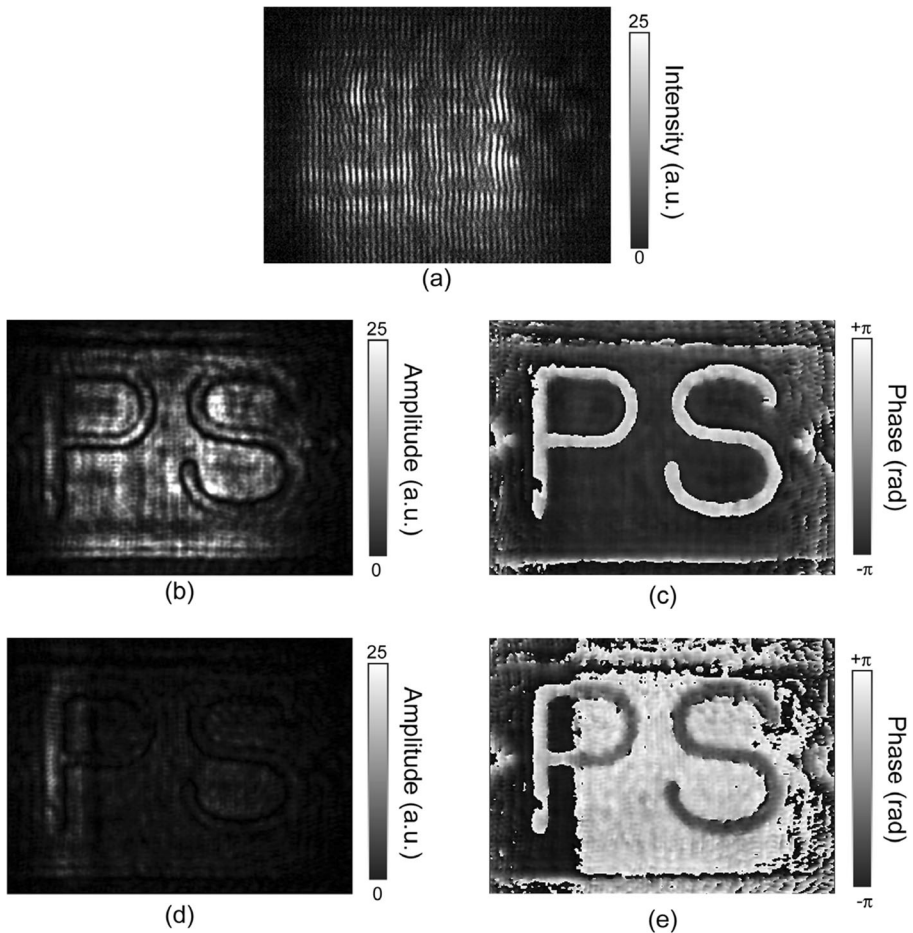
Fig. 4 Real-time movie of a visibly opaque, plastic sample. **a** Snapshot of a THz digital hologram (image size = 7.52 mm × 5.64 mm, pixel number = 320 pixels × 240 pixels, frame rate = 3.5 Hz). Snapshots of the reconstructed **b** amplitude and **c** phase movies (image size = 7.52 mm × 5.64 mm, pixel number = 320 pixels × 240 pixels) by ASM before the sample was screened by a paper sheet ($t = 0.285$ s). Snapshots of the reconstructed **d** amplitude and **e** phase movies (image size = 7.52 mm × 5.64 mm, pixel number = 320 pixels × 240 pixels) by ASM after the sample was screened by a paper sheet ($t = 1.710$ s). The corresponding movie is Video 2

We reconstructed a 3D image of the sample from the phase image, $\phi(x, y)$. The 2D distribution of the relative thickness, $t(x, y)$, was given by:

$$t(x, y) = \frac{\lambda}{2\pi\left(n_{sample} - n_{air}\right)} \phi(x, y), \tag{5}$$

where λ is the wavelength of the CW-THz radiation and n_{sample} and n_{air} are the refractive indices of the samples and air, respectively. n_{sample} was determined to be 3.1 by our asynchronous-optical-sampling terahertz time-domain spectrometer [22]. Figure 5e shows the $t(x, y)$ of the sample calculated from the phase image in Fig. 5d. The 3D contour of the sample was clearly visualized. Because the relative thickness was 13.4 ± 1.6 μm for the top
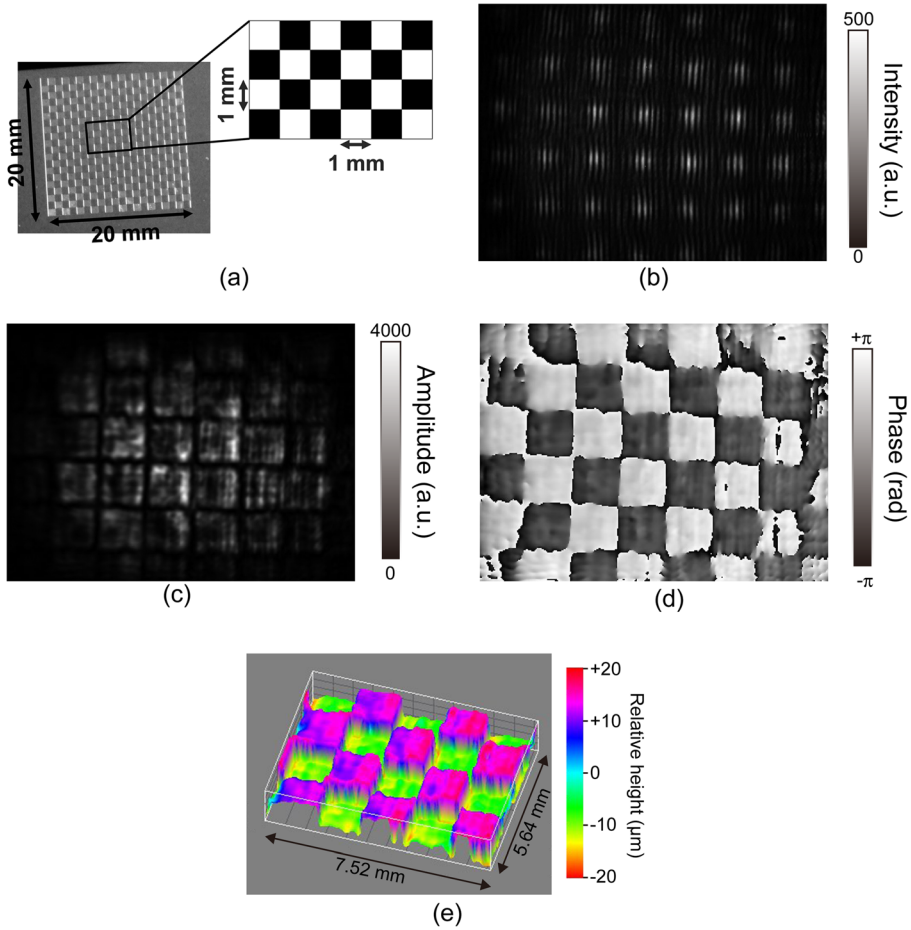
Fig. 5 **a** Optical photograph and schematic diagram of a visibly opaque, silicon sample with a checker pattern. **b** THz digital hologram (image size = 7.52 mm × 5.64 mm, pixel number = 320 pixels × 240 pixels, number of image integrations = 128). Reconstructed images of the **c** amplitude and **d** phase (image size = 7.52 mm × 5.64 mm, pixel number = 320 pixels × 240 pixels) by ASM. **e** 3D image calculated by the phase image in Fig. 5d

surface and -9.0 ± 1.8 μm for the bottom surface, the difference in the geometrical thickness was 22.4 ± 1.7 μm. This value is in good agreement with the value (21.11 ± 0.03 μm) obtained by 3D optical microscopy. The unevenness of the phase value in each pattern was due to the phase noise discussed later rather than the surface roughness of the sample. The expected values for the spatial resolution of the horizontal and vertical directions are given by:

$$SR_x = \frac{\lambda z}{M \Delta_x} = \frac{100 \times 10^{-6} \times 14 \times 10^{-3}}{320 \times 23.5 \times 10^{-6}} = 186 \text{ μm} \tag{6}$$

$$SR_y = \frac{\lambda z}{N \Delta_y} = \frac{100 \times 10^{-6} \times 14 \times 10^{-3}}{240 \times 23.5 \times 10^{-6}} = 248 \text{ μm}. \tag{7}$$
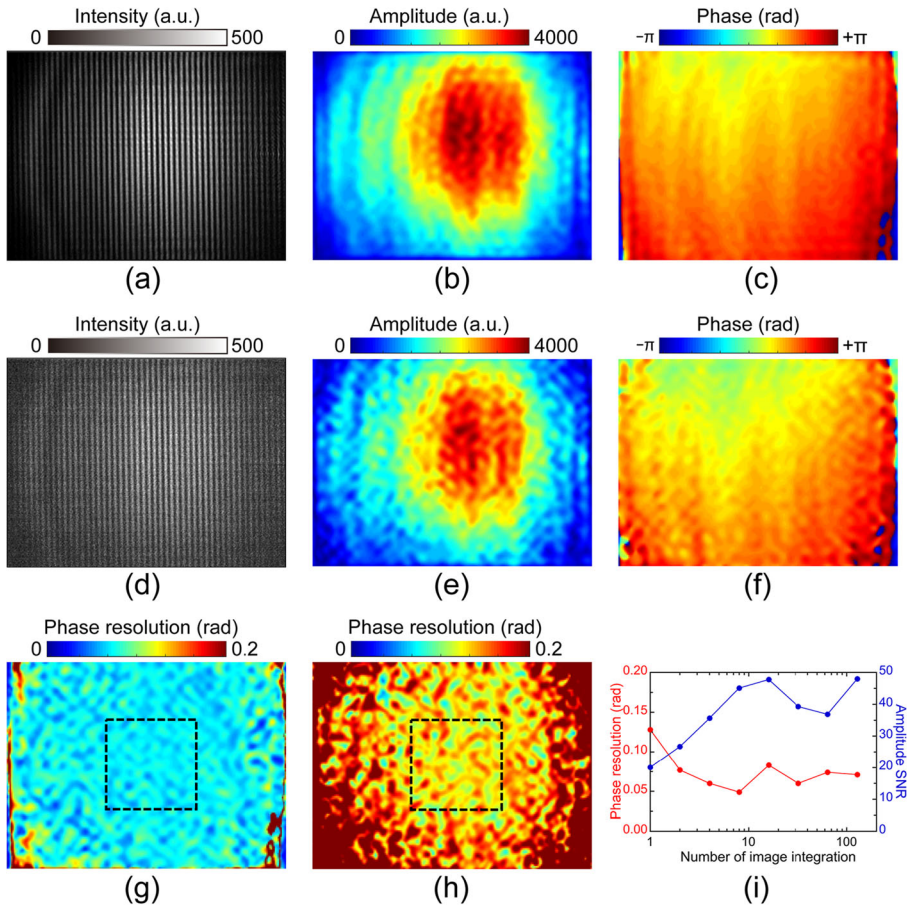
Fig. 6 **a** Thz digital hologram, **b** reconstructed amplitude image, and **c** reconstructed phase image without the sample (image size = 7.52 mm × 5.64 mm, pixel number = 320 pixels × 240 pixels, number of image integrations = 128). **d** THz digital hologram, **e** reconstructed amplitude image, and **f** reconstructed phase image without the sample (image size = 7.52 mm × 5.64 mm, pixel number = 320 pixels × 240 pixels, no image integrations). Spatial distribution of the phase noise in **g** 128-hologram-integrated and **h** no-hologram-integrated phase images. **i** Phase resolution and amplitude SNR with respect to number of image integration

4 Discussion

Phase resolution is an important performance of THz-DH to determine the depth precision of 3D imaging based on the phase image. Here, we discuss the phase resolution in the present phase image because the phase resolution is directly related to the depth resolution. The phase resolution is defined as the fluctuation of the phase value between different phase images, which depends on the robustness of the optical system to external disturbance (vibration, air turbulence, etc.) and/or SNR in the phase image. Figure 6a–c shows a typical hologram without the sample (image size = 7.52 mm × 5.64 mm, pixel number = 320 pixels × 240 pixels, number of image integrations = 128) and the corresponding amplitude and phase images (image size = 7.52 mm × 5.64 mm, pixel number = 320 pixels × 240 pixels), respectively. Also, Fig 6d–f shows the hologram, amplitude image, and the phase image when no image integrations were performed. Amplitude

images in Fig. 6b, e shows an uneven distribution of the amplitude value due to the beam profile of THz-QCL, which is in reasonable agreement with the bright distribution of holograms in Fig. 6a, d. In contrast, phase images in Fig. 6c, f shows significantly different profile from amplitude images in Fig. 6b, e. The mean and standard deviation of the spatial phase distribution were 1.44 ± 0.81 rad in Fig. 6c and 1.12 ± 0.75 rad in Fig. 6f, respectively.

We next evaluated the phase resolution using the phase image. To this end, we repeated 10 acquisitions of 128-hologram-integrated phase image and no-hologram-integrated phase image. Then, we calculated the standard deviation of the phase values at each pixel in 10 phase images to provide the phase resolution. Figure 6g, h shows the spatial distribution of the phase resolution for 128-hologram-integrated and no-hologram-integrated phase images (image size = 7.52 mm × 5.64 mm, pixel number = 320 pixels × 240 pixels). The spatial dependence of the phase resolution was relatively flat, and is related to the amplitude image because a decreased amplitude and the resulting low SNR increase the phase noise. The mean of the phase resolution in the whole image region of Fig. 6g was 0.10 rad, corresponding to a phase resolving power of $\lambda/62$; in the center region with a high SNR, as indicated by the black dashed box in Fig. 6g, the mean phase resolution and the corresponding phase resolving power were 0.071 rad and $\lambda/91$, respectively. From these values, the depth resolution in the 3D imaging was estimated to be 1.6 μm for the whole region and 1.1 μm for the center region. These estimated values are in reasonable agreement with the experimental values in Fig. 5e. On the other hand, the mean phase resolution and the corresponding phase resolving power in Fig. 6h were 0.071 rad and $\lambda/91$ for the whole region and 0.071 rad and $\lambda/91$ for the center region, respectively. These values determined the precision of the real-time phase imaging in Fig. 4 and Video 2. Finally, red plots in Fig. 6i shows dependence of the phase resolution on number of image integration. For comparison, blue plots in Fig. 6i shows a relation between amplitude SNR and number of image integration. These plots clearly indicate that the phase resolution depends on the amplitude SNR.

5 Conclusions

We constructed an off-axis THz-DH system equipped with THz-QCL and an uncooled, 2D micro-bolometer array, applied ASM to the acquired THz digital hologram, and performed real-time amplitude/phase imaging and digital focusing of visibly opaque objects. The quantitative phase imaging was confirmed by taking 3D imaging of these objects and evaluating the phase noise. The demonstrated real-time and precise 3D imaging capability will be a powerful tool for the non-destructive inspection of optically opaque soft materials.

References

1. U. Schnars, C. Falldorf, J. Watson, W. Jüptner, Digital holography (Springer Berlin, 2005).
2. P. Langehanenberg, G. von Bally, B. Kemper, 3D Res. 2, 4 (2011).
3. B. Kemper, G. Bally, Appl. Opt. 47, A52 (2008).
4. B. Javid, E. Tajahuerce, Opt. Lett. 25, 610 (2000).
5. M. Tonouchi, Nat. Photonics 1, 97 (2007).
6. D. M. Mittleman, Sensing with THz radiation (Springer, 2003).
7. M. S. Heimbeck, M. K. Kim, D. A. Gregory, H. O. Everitt, Opt. Express 19, 9192 (2011).
8. S. Ding, Q. Li, Y. Li, Q. Wang, Opt. Lett. 36, 1993 (2011).
9. K. Xue, Q. Li, Y. Li, Q. Wang, Opt. Lett. 37, 3228 (2012).
10. E. Hack, P. Zolliker, Opt. Express 22, 16079 (2014).
11. L. Rong, T. Latychevskaia, D. Wang, X. Zhou, H. Huang, Z. Li, Y. Wang, Opt. Express 22, 17236 (2014).
12. L. Rong, T. Latychevskaia, C. Chen, D. Wang, Z. Yu, X. Zhou, Z. Li, H. Huang, Y. Wang, Z. Zhou, Sci. Reports 5, 8445 (2015).
13. M. Locatelli, M. Ravaro, S. Bartalini, L. Consolino, M. S. Vitiello, R. Cicchi, F. Pavone, P. De Natale, Sci. Reports 5, 13566 (2015).
14. H. Zolliker, E. Hack, Opt. Express 23, 10957 (2015).
15. M. S. Heimbeck, W.-R. Ng, D. R. Golish, M. E. Gehm, H. O. Everitt, IEEE Trans. THz Sci. Technol. 5, 110 (2015).
16. L. Valzania, P. Zolliker, E. Hack, Opt. Express 25, 11038 (2017).
17. B. S. Williams, Nat. Photon. 1, 517 (2007).
18. S. Kumar, IEEE J. Sel. Top. Quantum Electron. 17, 38 (2011).
19. N. Oda, C. R. Phys. 11, 496 (2010).
20. M. K. Kim, L. Yu, C. J. Mann, J. Opt. A: Pure Appl. Opt. 8, S518 (2006).
21. T. C. Poon, J. P. Liu, Introduction to modern digital holography with MATLAB (Cambridge University Press, 2014).
22. Y.-D. Hsieh, S. Nakamura, D. G. Abdelsalam, T. Minamikawa, Y. Mizutani, H. Yamamoto, T. Iwata, F. Hindle, T. Yasui, Sci. Reports 6, 28114 (2016).